Langmuir

ARTICLE

pubs.acs.org/Langmuir

Enhanced Stability of Janus Nanoparticles by Covalent Cross-Linking of Surface Ligands

Yang Song,[†] Liana M. Klivansky,[‡] Yi Liu,[‡] and Shaowei Chen*[,†]

[†]Department of Chemistry and Biochemistry, University of California, 1156 High Street, Santa Cruz, California 95064, United States

[‡]The Molecular Foundry, Lawrence Berkeley National Laboratory, One Cyclotron Road, Berkeley, California 94720, United States

Supporting Information

ABSTRACT: A mercapto derivative of diacetylene was used as the hydrophilic ligand to prepare Janus nanoparticles by using hydrophobic hexanethiolate-protected gold (AuC6, diameter 5 nm) nanoparticles as the starting materials. The amphiphilic surface characters of the Janus nanoparticles were verified by contact angle measurements, as compared to those of the bulk-exchange counterparts where the two types of ligands were distributed rather homogeneously on the nanoparticle surface. Dynamic light scattering studies showed that the Janus nanoparticles formed stable superstructures in various solvent media that were significantly larger than those by the bulk-exchange counterparts. This was ascribed to the amphiphilic characters of the Janus nanoparticles that rendered the particles to behave analogously to conventional surfactant molecules. Notably, because of the close proximity of the diacetylene moieties on the Janus nanoparticle surface, exposure to UV irradiation led to effective covalent cross-linking between the diacetylene moieties of neighboring ligands, as manifested in UV−vis and fluorescence measurements where the emission characteristics of dimers and trimers of diacetylene were rather well-defined, in addition to the monomeric emission. In contrast, for bulk-exchange nanoparticles, no trimer emission could be identified, and the intensity of dimer emission was markedly lower (though the intensity increased with increasing diacetylene coverage on the particle surface) under the otherwise identical experimental conditions. This is largely because the diacetylene ligands were distributed on the entire particle surface, and it was difficult to find a large number of ligands situated closely so that the stringent topochemical principles for the polymerization of diacetylene derivatives could be met. Importantly, the cross-linked Janus nanoparticles were found to exhibit marked enhancement of the structural integrity, which was attributable to the impeded surface diffusion of the thiol ligands on the nanoparticle surface, as manifested in fluorescence measurements of aged nanoparticles.

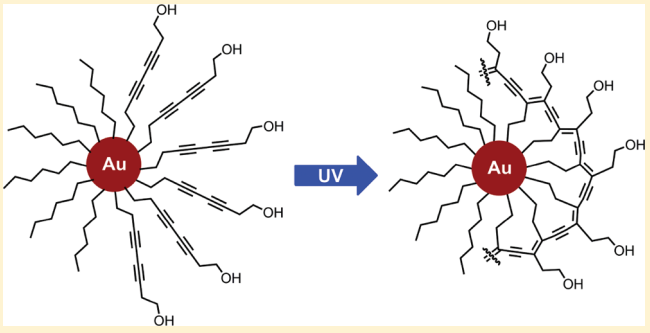

INTRODUCTION

Nanoparticles have attracted increasing attention because of their potential application as novel building blocks for the fabrication of next-generation optical/electronic devices. This is attributed to their unique material properties that are vastly different from those of their constituent atoms or bulk forms.[1−4] Yet, to exploit these unprecedented material properties, it becomes critically important to search for additional material design parameters beyond the conventional variables of size and shape. Toward this end, preparation of amphiphilic Janus nanoparticles has represented an attractive route. Actually, it was Casagrande and co-workers who first created the term "Janus beads" to denote partial hydrophobic modification of commercial glass spheres.[5,6] Janus particles refer to a class of nanoparticle materials that exhibit hydrophobic characters on one side and hydrophilic characters on the other, akin to the Roman god, Janus. Because of their asymmetrical surface chemistry, the nanoparticles behave analogously to conventional surfactant molecules and thus may be exploited in the formation of functional superstructures by virtue of controlled self-assembly.

Previously, we developed two effective approaches based on interfacial engineering for the preparation of nanosized Janus particles.[7−11] In both routes, alkanethiolate-protected gold nanoparticles were used as the starting materials. In the first method,[7] a particle monolayer was formed at the air−water interface by the Langmuir method. At sufficiently high surface pressures, intercalation of the protecting ligands between neighboring particles occurred, leading to impeded interfacial mobility of the nanoparticles. At this point, injection of a calculated amount of hydrophilic thiol derivatives (e.g., 1,2-mercaptopropanediol, MPD) into the water subphase led to ligand-exchange reactions that were confined to the bottom

Received: August 19, 2011
Revised: October 4, 2011
Published: October 17, 2011

face of the nanoparticles and, hence, to the production of Janus nanoparticles. In the second method,[9] the nanoparticle monolayer was first transferred onto a glass slide by the Langmuir–Blodgett (LB) method and then was immersed into a water (or ethanolic) solution containing the hydrophilic thiol ligands (e.g., 2-(2-mercaptoethoxy)ethanol, MEA). As the nanoparticles were tightly arranged on the substrate surface, ligand-exchange reactions were limited to the top side of the nanoparticles, resulting in asymmetrical functionalization of the nanoparticles. The amphiphilic nature of these nanoparticles was then examined by contact angle, adhesion force microscopy, nuclear Overhauser enhancement spectroscopy (NOESY) NMR, and other spectroscopic measurements, and the particles were found to form stable superstructures in appropriate solvent media, similarly to conventional surfactant molecules, as manifested in dynamic light scattering, transmission electron microscopy, and atomic force microscopy studies.[7−11] The asymmetrical surface chemistry has also been exploited for further chemical functionalization, as demonstrated by the preparation of Au-TiO_2 heterodimers that serve as an effective photocatalyst for the oxidation of methanol to formaldehyde.[10]

However, it has been well-known that thiol molecules exhibit rather apparent lateral diffusion on gold surfaces even at ambient temperature, which might be driven entropically, as manifested in the diminishment of domain segregation between thiol ligands with different functional moieties.[12,13] In fact, the Janus nanoparticles prepared above appeared to lose the amphiphilic characters after an extended period of time in solution, with the final structure similar to that of the particles that underwent ligand-exchange reactions in a solution (rather than at an interface) with the same hydrophilic ligands (the so-called bulk-exchange particles).[9] This indicates that a rather homogeneous mixing was reached eventually between the hydrophobic and hydrophilic ligands on the Janus nanoparticle surface, most probably as a consequence of ligand lateral diffusion on the nanoparticle surface (additional contribution may arise from ligand hopping between particles[13]). Such an observation presents a great challenge in the further functionalization and utilization of the Janus nanoparticles. Thus, it becomes imperative to develop effective protocols to enhance the structural integrity of the Janus nanoparticles, one of which is to covalently cross-link the nanoparticle surface ligands. This is the primary motivation of the present study.

Herein, using the protocols that we developed earlier,[7−11] we prepared Janus nanoparticles with 1-hexanethiolates on the hydrophobic side and with 3,5-octadiyne-1-ol-8-thiol (DAT) as the hydrophilic ligands, where photopolymerization of the diacetylene moieties was exploited for covalent cross-linking between the surface ligands and, hence, for enhanced structural stability of the Janus nanoparticles. It has been demonstrated that polymerization of diacetylene derivatives has to abide by topochemical principles.[14−16] In fact, effective photopolymerization has been observed with mercapto derivatives of diacetylene self-assembled on gold surfaces, regardless of the vertical position of the diacetylene moieties within the molecular backbones.[17] On gold nanoparticle surfaces, apparent photopolymerization also occurs; yet, the polydiacetylene phase (or the degree of polymerization) has been found to depend critically on the particle core size as well as on the exact location of the diacetylene moieties within the ligand structures, most probably because of the nanoscale curvatures of the metal cores and the resulting diminishment of ligand-packing density along the radial direction.[18]

Scheme 1. Synthetic Procedure of DAT

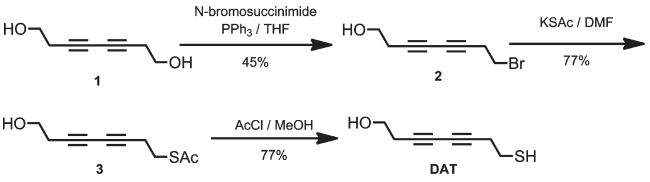

In the present study, we demonstrated that the diacetylene moieties on the Janus nanoparticles could also be effectively photopolymerized and that the extent of polymerization was markedly greater than that observed with the bulk-exchange counterparts at similar diacetylene surface concentration, leading to marked enhancement of the Janus nanoparticle structural integrity.

EXPERIMENTAL SECTION

General Method. Reagents were purchased from commercial sources as noted or were synthesized as described. Thin-layer chromatography (TLC) was carried out using aluminum sheets precoated with silica gel 60F (Merck 5554). The plates were inspected by UV light. Proton and carbon nuclear magnetic resonance spectra (^{1}H and ^{13}C NMR) were recorded on a Bruker Avance 500 II using the deuterated solvent as lock and tetramethylsilane as internal standard. All chemical shifts are quoted using the δ scale, and all coupling constants (J) are expressed in Hz.

Hydrogen tetrachloroauric acid ($HAuCl_4 \cdot xH_2O$) was synthesized by dissolving ultrahigh purity gold (99.999%, Johnson Matthey) in freshly prepared aqua regia followed by crystallization.[19] Tetraoctylammonium bromide (Alfa Aesar, 98%), 1-hexanethiol (C6SH, Acros, 96%), and sodium borohydride ($NaBH_4$, Acros, 99%) were all used as received. Solvents were purchased from typical commercial sources at their highest purity and were used without further treatments. Water was supplied by a Barnstead Nanopure water system (18.3 MΩ·cm).

The DAT ligand was synthesized in three steps as described in Scheme 1. Bromination of 3,5-dioctadiyn-1,8-diol (**1**) using 1 equiv of *N*-bromosuccinimide and triphenylphosphine gave the monobromide **2** in 45% yield, which was transformed into the corresponding thioacetate **3** in 77% yield after treating with potassium thioacetate in dimethylformamide (DMF) at room temperature. A mild hydrolysis condition using acetyl chloride and methanol was employed to convert **3** into DAT in 77% yield.

Synthesis of 8-Bromo-3,5-dioctadiyn-1-ol (2). To the suspension of 3,5-dioctadiyn-1,8-diol (**1**) (2.00 g, 14.5 mmol, 1.00 equiv) in tetrahydrofuran (THF) (240 mL) at 0 °C was added PPh_3 (4.06 g, 15.5 mmol, 1.07 equiv). After 15 min, *N*-bromosuccinimide (NBS) (2.58 g, 14.5 mmol, 1.00 equiv) was added to the mixture. The reaction was stirred at room temperature for 2 days. The suspension was filtered, and the filtrate was evaporated to give an oil, which was subjected to column chromatography (silica gel, ethyl acetate/hexanes 1:1) to afford **2** as a colorless oil which slowly solidified upon standing (1.31 g, 45%). ^{1}H NMR ($CDCl_3$, 298 K, 500 MHz): δ (ppm) 3.78 (t, J = 6.5 Hz, 2 H), 3.46 (t, J = 7.0 Hz, 2 H), 2.86 (tt, J = 7.0 Hz, 1.0 Hz, 2 H), 2.57 (tt, J = 6.5 Hz, 1.0 Hz, 2 H).

Synthesis of 8-Thioacetate-3,5-dioctadiyn-1-ol (3). A mixture of bromide **2** (1.00 g, 4.97 mmol, 1.00 equiv) and potassium thioacetate (0.568 g, 4.97 mmol, 1.00 equiv) in DMF (100 mL) was stirred overnight at room temperature. After the solvent was removed

Scheme 2. Formation of Janus Nanoparticles Based on Interfacial Exchange Reactions of AuC6 Nanoparticles with DAT Ligands

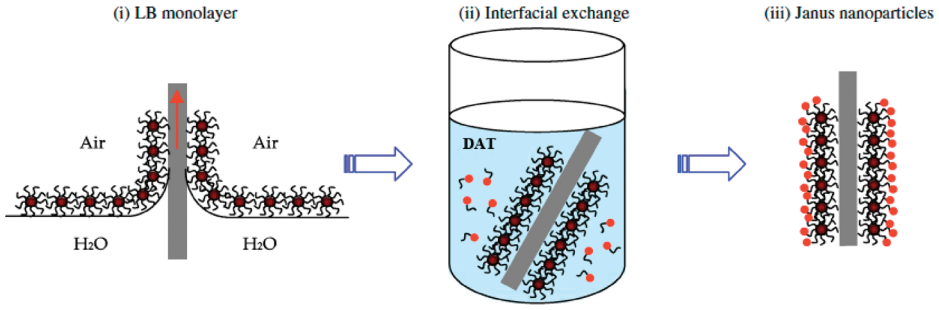

under reduced pressure, the residue was partitioned in a CH_2Cl_2/H_2O mixture. The aqueous layer was further extracted twice with CH_2Cl_2, and the organic layers were combined, were dried over $MgSO_4$, and were concentrated. The residue was then subjected to column chromatography (silica gel, ethyl acetate/hexanes 1:1) to give **3** as a white solid (0.750 g, 77%). ^{1}H NMR ($CDCl_3$, 298 K, 500 MHz): δ (ppm) 3.77 (q, J = 6.3 Hz, 2 H), 3.04 (t, J = 7.0 Hz, 2 H), 2.56 (qt, J = 7.0 Hz, 1.0 Hz, 4 H), 2.37 (s, 3 H), 1.75 (t, J = 6.3 Hz, 1 H). ^{13}C NMR ($CDCl_3$, 298 K, 125 MHz): δ (ppm) 195.3, 75.4, 74.8, 66.6, 66.3, 60.8, 30.6, 27.9, 23.7, 20.3 HR-MS (EI): $[M]^+$ calcd for $C_{10}H_{12}O_2S$: 196.0558, found: 196.0565 (100%).

Synthesis of DAT. A mixture of acetate **3** (102 mg, 0.520 mmol, 1.00 equiv) and acetyl chloride (22 μL, 0.572 mmol, 1.11 equiv) in methanol (500 μL) was stirred at room temperature for 2 days. The solvent was removed under reduced pressure, and the residue was subjected to column chromatography (silica gel, ethyl acetate/hexanes 1:1) to give DAT as a white solid (62 mg, 77%). ^{1}H NMR ($CDCl_3$, 298 K, 500 MHz): δ (ppm) 3.78 (t, J = 6.3 Hz, 2 H), 2.70 (m, 2 H), 2.63 (t, J = 7.0 Hz, 2 H), 2.57 (t, J = 6.3 Hz, 2 H), 1.73 (m, 2 H). ^{13}C NMR ($CDCl_3$, 298 K, 125 MHz): δ (ppm) 75.4, 74.9, 66.8, 66.8, 60.8, 24.6, 23.6, 23.5 HR-MS (EI): $[M]^+$ calcd for $C_8H_{10}OS$: 154.0452, found: 154.0457 (100%).

Gold Janus Nanoparticles. 1-Hexanethiolate-protected gold (AuC6) nanoparticles were prepared by adopting the Brust method[20] and were separated into different fractions by using a mixed solvent of toluene and ethanol.[21] The fraction with an average core diameter of about 5 nm was then used for the preparation of Janus nanoparticles by taking advantage of the interfacial place exchange reactions of the AuC6 nanoparticles with the DAT ligands.[9] The procedure is depicted in Scheme 2. First, a monolayer of the AuC6 nanoparticles was deposited by the Langmuir−Blodgett technique onto a clean glass slide surface at a sufficiently high surface pressure where ligand intercalation between neighboring nanoparticles occurred (step i). The surface area of the glass slide was typically 8 cm × 3 cm. The glass substrate with the deposited particle monolayer was then immersed into an ethanolic solution of 1 mM DAT (step ii). It is anticipated that the exchange reactions of the AuC6 particles with the DAT ligands only took place at the top face of the particles that was in direct contact with the ethanol phase and, hence, the generation of Janus nanoparticles (step iii). At varied immersion time intervals, the glass slide was taken out of the DAT solution, was gently rinsed with copious amounts of ethanol to remove excessive DAT and displaced hexanethiolate ligands, was dried in a gentle stream of ultrahigh-purity nitrogen, and then was subject to contact angle measurements (see below) before being collected into a vial by chloroform. At least four batches of particle samples were prepared and collected under identical conditions so that there were enough materials for further analyses. The resulting Janus particles were found to be soluble in chloroform and THF.

As a control measurement, exchange reactions of the AuC6 nanoparticles with DAT were also carried out by mixing a calculated amount of AuC6 nanoparticles and DAT ligands in THF and were stirred for 48 h. The solution was then dried under reduced pressure with a rotary evaporator, and excessive ligands were removed by extensive rinsing with methanol. The resulting particles were denoted as bulk-exchange (BE) particles and, similar to the Janus nanoparticles, were soluble in chloroform and THF. Three bulk-exchange nanoparticles were prepared at different loadings of DAT on the nanoparticle surface, which were denoted as BE-1, BE-2, and BE-3 (vide infra).

Polymerization of the diacetylene moieties on the resulting Janus and BE nanoparticle surface was carried out by exposing the respective particle solution at a concentration of ca. 0.5 mg/mL in THF in a 1 cm quartz cuvette to a low-intensity UV lamp (model UVGL-58; Ultra-Violet Products Inc.; λ = 254 nm) at a distance of 2 cm for 30 min.

Contact Angle Study. Contact angles were measured with a Tantec CAM-PLUS contact angle meter. For the BE nanoparticles, the contact angles were measured with their monolayers deposited onto a clean glass slide surface by the Langmuir−Blodgett method at the same surface pressures where Janus nanoparticles were prepared. For self-assembled monolayers of hexanethiol, DAT, and their mixture, the samples were prepared by immersing a clean Au thin film on a glass slide into an ethanolic solution (1 mM) of the respective thiol for about 24 h. For each sample, at least eight independent measurements were carried out for statistical analyses.

Spectroscopy. The UV−vis spectra were collected with a UNICAM ATI UV4 spectrometer at a particle concentration of 0.5 mg/mL in THF using a 1 cm quartz cuvette. ^{1}H NMR spectra were collected by using a Varian Oxford 600 MHz spectrometer. The particles were dissolved in $CDCl_3$ at a concentration of ca. 1 mg/mL. The absence of sharp features in NMR measurements was used to confirm the removal of excessive ligands in the nanoparticle samples. In addition, the ratio between the integrated peak areas of the methyl protons (CH_3, hexanethiolate) and the methylene protons next to the hydroxy group (CH_2OH, DAT) was exploited for the determination of the DAT coverage on the nanoparticle surface, which is summarized in Table 1 (the corresponding NMR spectra are included as Figure S1 in the Supporting Information): Janus, 51.86%; BE-1, 24.40%; BE-2, 57.20%; and BE-3, 73.21%.

Dynamic Light Scattering (DLS). Dynamic light scattering (DLS) measurements were carried out by using a Protein Solution Dynapro temperature controlled microsampler with the nanoparticles dissolved in varied solvent media. The particles were initially dissolved in THF, and an equal amount of water was then added into the solution. THF was then removed by bubbling nitrogen to afford water solutions of the nanoparticle samples. An aliquot (12 μL) of the particle solutions at a concentration of ca. 0.05 mg/mL was introduced into a sample holder using a 20 μL micropipet. The results were reported in terms of %mass.

RESULTS AND DISCUSSION

To confirm the amphiphilic character of the resulting Janus nanoparticles, the contact angle of the nanoparticle monolayers

Table 1. DAT Coverage on the Nanoparticle Surface and Contact Angles of Janus and BE Nanoparticles and of Self-Assembled Monolayers (SAMs) of C6SH, DAT, and Their Mixture

sample	DAT coverage (%)	contact angle
AuC6/Janus nanoparticles	51.86[a]	63.4° ± 0.8° (0 h) 52.8° ± 1.4° (8.5 h)
BE-1 nanoparticles	24.40	60.1° ± 1.0°
BE-2 nanoparticles	57.20	58.0° ± 0.9°
BE-3 nanoparticles	73.21	55.3° ± 1.4°
C6 SAM		62.8° ± 0.9°
DAT SAM		52.6° ± 1.0°
C6-DAT (1:1) mixed SAM		57.3° ± 1.3°

[a] Obtained from the samples collected after 8.5 h of exchange reactions (Figure 1).

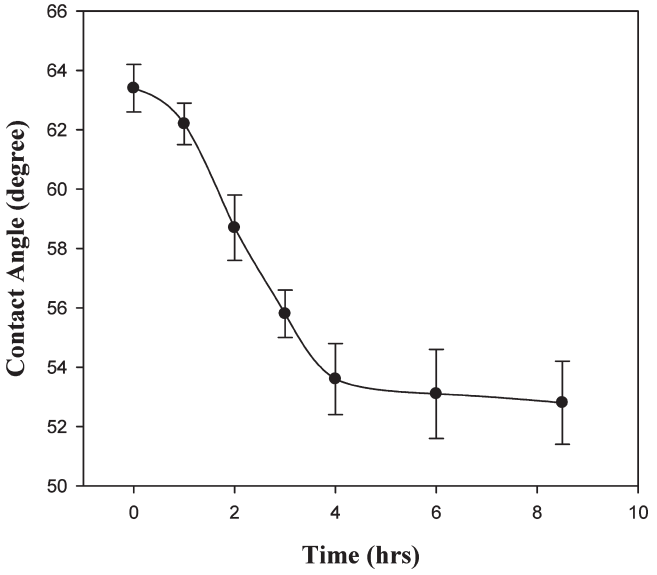

Figure 1. Contact angles of a Langmuir−Bloggett monolayer of AuC6 nanoparticles after being immersed in 1 mM DAT in ethanol at room temperature for different periods of time.

was monitored at different immersion time intervals (step ii). The result is depicted in Figure 1. It can be seen that prior to the immersion of the nanoparticle monolayers into the DAT solution (i.e., at t = 0 h), the contact angle of the AuC6 nanoparticle film was 63.4° ± 0.8°, and it decreased slightly to 62.2° ± 0.7° after one hour of exchange reactions. Further immersion led to a more rapid decrease of the contact angle, and at t = 4 h, it dropped drastically to 53.6° ± 1.2°. Yet, it remained statistically invariant thereafter (52.8° ± 1.4° at 8.5 h). The observed evolution of the contact angle of the nanoparticle LB monolayers with immersion time might be accounted for by the nanocrystalline morphology of the nanoparticles, where ligand place exchange reactions on alkanethiolate-protected gold nanoparticles presumably start with the surface defect sites (e.g., edges and vertices) and then propagate to the terrace sites.[22−24] That is, the small decrease of contact angle within the first hour is likely a consequence of the initial phase of exchange reactions involving surface defects, whereas the more significant drop of contact angles at 4 h arises from the incorporation of hydrophilic DAT ligands onto the more populous terrace sites on the particle surface. The almost constant contact angle after 4 h seems to suggest that the exchange reaction has reached an equilibrium. Similar behaviors were observed previously with 2-(2-mercaptoethoxy)-ethanol (MEA) as the hydrophilic ligands.[9]

The contact angles of the self-assembled monolayers of C6SH and DAT on flat gold thin film surfaces were 62.8° ± 0.9° and 52.6° ± 1.0°, respectively (Table 1). These are very consistent with those observed with the original AuC6 nanoparticles (t = 0 h) and the Janus nanoparticles (t = 8.5 h) as depicted in Figure 1, again supporting the notion that the top face of the nanoparticle monolayers indeed underwent effective ligand-exchange reactions. In addition, experimentally, we observed no loss of nanoparticles into the ethanol solution during the entire experimental procedure, which implies that not all the original hydrophobic ligands (hexanethiolates) were replaced by the hydrophilic DAT ligands. This may be ascribed to the inaccessibility of the bottom face of the nanoparticles by the DAT ligands because of ligand intercalation, which impeded interfacial mobility of the nanoparticles on the substrate surface and, hence, led to the formation of asymmetrically functionalized nanoparticles.[9]

Further control experiments were carried out with the BE nanoparticles. As manifested previously,[7−11] the DAT ligands were anticipated to be incorporated rather homogeneously onto the particle surface during bulk-exchange reactions, and thus, the contact angles of the BE particle monolayers should be in the intermediate range between those observed with Janus nanoparticles and those of the original AuC6 nanoparticles and decreased with increasing DAT coverage. In fact, the contact angles were 60.1° ± 1.0°, 58.0° ± 0.9°, and 55.3° ± 1.4° for the LB monolayers of BE-1, BE-2, and BE-3 nanoparticles, respectively (Table 1). Notably, for BE-2 that exhibited a DAT coverage of 57.20%, the contact angle was similar to that observed with a mixed self-assembled monolayer (SAM) of C6SH and DAT (molar ratio 1:1) on a gold film surface, 57.3° ± 1.3°, indeed suggestive of a homogeneous mixing of the ligands on the BE nanoparticle surfaces.

The amphiphilic structure of the Janus nanoparticles was further manifested in the formation of stable nanoparticle superstructures in selected solvent media, as examined by dynamic light scattering (DLS) measurements, in comparison with the bulk-exchange counterparts. Table 2 lists the size of the aggregates of the Janus and BE nanoparticles in different solvents. It can be seen that the Janus nanoparticles formed stable aggregates when dispersed in THF, with the average radius of the aggregates at 327.0 nm. With the addition of an equal amount of water into the THF solution, the size of the aggregates increased to 404.0 nm; when THF was removed from the solution by nitrogen bubbling, the aggregates shrank

Table 2. Average Size of Particle Aggregates in Different Solvents by DLS Measurements

solvent	Janus particles (nm)	BE-1 particles (nm)	BE-2 particles (nm)	BE-3 particles (nm)
THF	327.0	8.4	98.0	95.4
THF/H_2O (50:50)	404.0	58.7	6.8	47.4
H_2O	312.0	105.0	115.0	96.1

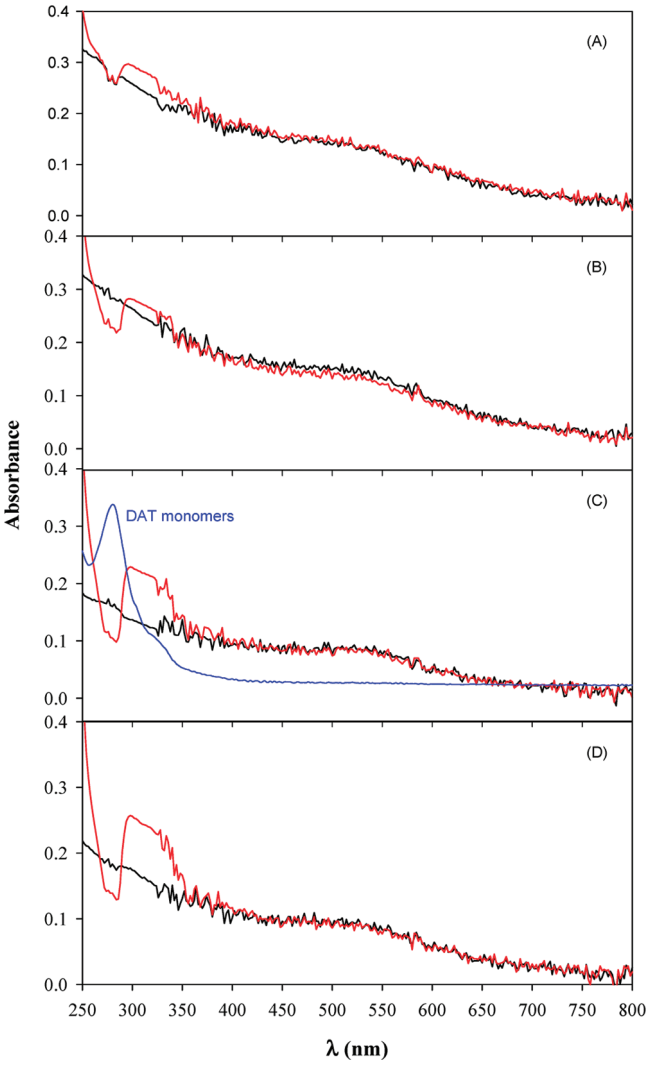

Figure 2. UV−vis spectra of (A) BE-1, (B) BE-2, (C) BE-3, and (D) Janus nanoparticles before (black) and after (red) UV exposure. The particle concentrations were all ca. 0.5 mg/mL in THF. The absorption spectrum of monomeric DAT in THF was also included (blue curve in panel C).

somewhat to 312.0 nm. These observations suggest that stable aggregates of Janus nanoparticles were formed in these three solvent media of different polarity, most likely because of the amphiphilic character of the nanoparticle surface that rendered it energetically favorable for the nanoparticles to form (reverse-)-micelle-like superstructures.

The behaviors were drastically different with the BE nanoparticles. When dispersed in THF, BE-1 nanoparticles exhibited a very low degree of aggregation with the average radius of the aggregates at 8.4 nm (the physical diameter of the nanoparticles, gold core plus two fully extended ligands, is about 6.5 nm), most probably because the low concentration of DAT on the nanoparticle surface rendered the particles soluble in relatively apolar organic solvents, whereas for BE-2 and BE-3 nanoparticles that exhibited a higher concentration of DAT on the nanoparticle surface, the aggregates were much larger at 98.0 and 95.4 nm, respectively. However, in a THF/water mixture (1:1 v:v), the BE-2 nanoparticles behaved as individual nanoparticles with the measured size of 6.8 nm, whereas BE-1 and BE-3 nanoparticles were found to form aggregates of 58.7 and 47.4 nm, respectively. This seems to suggest that the polarity of the mixed solvent media was compatible with that of the BE-2 nanoparticles that featured a mixed monolayer of approximately 1:1 ratio between the hydrophobic and the hydrophilic ligands. In pure water, however, the three BE nanoparticles formed aggregates with sizes all close to 100 nm.

One can see that in any of the solvent media under study, the Janus nanoparticles were able to form much larger stable aggregates, and the size of the aggregates only fluctuated slightly with the polarity of the solvents. This is, again, most probably attributable to the amphiphilic nature of the particles that rendered it energetically favorable to arrange the particles in response to the solvent media, analogously to conventional surfactant molecules that have been found to form micelles or reverse-micelles depending on the solvent polarity. Such responsive arrangements of the nanoparticles cannot be achieved with bulk-exchange nanoparticles where the hydrophilic and hydrophobic ligands were mixed rather homogeneously on the entire nanoparticle surface.

The incorporation of the DAT ligands onto the nanoparticle surface rendered the nanoparticles photoactive. Yet, because of the drastic difference in the way the DAT ligands were distributed on the Janus and BE nanoparticle surfaces, there was substantial discrepancy in the resulting optical characteristics. In UV−vis absorption measurements, as depicted in the black curves of Figure 2, both Janus (panel D) and BE (panels A−C) nanoparticles exhibited an exponential decay response with a small and broad peak at ca. 520 nm that was characteristic of the surface plasmon resonance of nanosized gold particles.[21,25,26] Additionally, a small absorption band appeared at around 280 nm, which is consistent with the absorption profile of monomeric DAT ligands (blue curve in panel C). In fact, the peak became increasingly apparent with increasing DAT coverage on the nanoparticle surface (from BE-1 to BE-3 nanoparticles) as shown in panels A−C.

UV irradiation (λ = 254 nm) was then exploited to initate covalent cross-linking of the diacetylene moieties between neighboring particle-bound ligands (Scheme 3), and the UV−vis absorption spectra were shown as the respective red curves in the figure. One can see that a fairly broad and yet well-defined peak now started to emerge within the range of 280 and 350 nm, which most probably arose from the resulting oligomers of the diacetylene moieties.[27,28] Furthermore, the intensity of this peak actually increases with increasing DAT coverage on the nanoparticle surface (from BE-1 to BE-3 nanoparticles in panels

dx.doi.org/10.1021/la2032626 |*Langmuir* 2011, 27, 14581–14588

Scheme 3. Photopolymerization of the Diacetylene Moieties of the Janus Nanoparticles (Not to Scale; Actual Extent of Polymerization Varies)

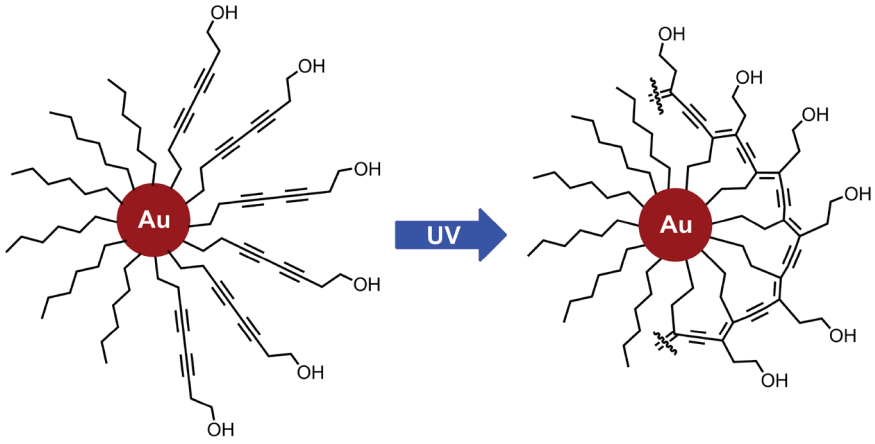

A−C). Interestingly, the peak intensity of the Janus nanoparticles appeared to be the greatest (panel D), although the DAT coverage was only comparable to that on BE-2 nanoparticles, implying that the efficiency of covalent cross-linking between the diacetylene moieties on the Janus nanoparticles was much greater than that on the BE nanoparticles, most probably as a result of the close proximity between the DAT ligands.[14−16]

In contrast, in the longer wavelength region, the absorption profiles were essentially the same as those before UV exposure (black curves). In previous studies, it has been shown that the carbon backbone of fully conjugated polydiacetylene (PDA) is planar, and the lowest energy optical transition ($\pi-\pi^*$) is located at about 620 nm.[27,28] However, distortion of the conjugated carbon backbone because of disorder or strain may reduce the extent of orbital overlap and, hence, the average conjugation length. Therefore, the $\pi-\pi^*$ transition might shift to a higher energy (~540 nm) and render the polymer to appear red. For the Janus and BE nanoparticles in the present study, only a small number of DAT ligands on the spherical surface of the gold cores are likely to satisfy the stringent topological requirements for polymerization. Thus, it is most probable that the red-form absorption would dominate. This frequency happens to coincide with the surface plasmon absorption of the gold nanoparticles and, hence, becomes difficult to be distinguishable.[29] Similar behaviors have been observed previously. For instance, Kanaras and Bartczak[30] prepared gold nanoparticles (diameter 15.0 and 3.25 nm) stabilized by a full monolayer of thiol ligands with a diacetylene-oligo(ethylene glycol) conjugate. Photopolymerization of the diacetylene moieties produced no apparent variation of the corresponding UV−vis absorption profiles (except for a slight sharpness of the nanoparticle surface plasmon resonance).

Notably, both the Janus and the BE nanoparticles exhibited apparent fluorescence that was characteristic of polymerized diacetylene moieties, although the extent of polymerization on the Janus nanoparticles differed markedly from that on the BE nanoparticles, as the oligomers of diacetylene have been known to exhibit distinctly different fluorescence emissions depending on the conjugation length.[31,32] Prior to UV exposure, both the Janus and the BE nanoparticles in solutions showed only one emission peak at λ_{em} = 419 nm when excited at λ_{ex} = 366 nm (solid curves); excitation at other wavelength positions did not lead to any apparent emission (dotted and dashed curves), as depicted in Figure 3A. This is characteristic of the fluorescence of monomeric diacetylene moieties. Interestingly, after exposure to UV light (λ = 254 nm) for 30 min, besides the emission at λ_{em} = 419 nm (solid black curves), the solution of the Janus nanoparticles showed two additional well-defined emissions at longer wavelength positions, λ_{em} = 445 nm (when excited at λ_{ex} = 401 nm, dotted black curves) and λ_{em} = 484 nm (at λ_{ex} = 430 nm, dashed black curves), as shown in Figure 3B. These fluorescence characteristics are very analogous to those observed with monomers, dimers, and trimers of the diacetylene moieties in two-dimensional self-assembled monolayer of diactylene derivatives.[31] This suggests that a mixture of monomers, dimers, and trimers was produced after the Janus nanoparticles were exposed to UV irradiation. In contrast, no trimers of the diactylene moieties were found when the BE nanoparticles were exposed to the same UV irradiation, and the fluorescence emission could only be ascribed to monomers and dimers. For instance, after UV exposure, BE-1 nanoparticles exhibited two emissions at λ_{em} = 419 nm (monomers, solid green curves) and 445 nm (dimers, dotted green curves), and no trimer emission was observed at 484 nm (dashed green curves). For BE-2 nanoparticles where the surface coverage of DAT ligands increased to 57.20%, the intensity of the dimer emission increased slightly while the trimer emission was still absent (red curves). With a further increase of the DAT surface coverage to 73.21% (BE-3 nanoparticles, blue curves), the dimer emission exhibited a further enhancement, and the trimer emission (λ_{em} = 484 nm) now started to emerge.

The discrepancy observed above between the fluorescence characterictics of the Janus and BE nanoparticles may be ascribed to the difference of the DAT ligand distributions on the nanoparticle surface. For the Janus nanoparticles, the DAT ligands were concentrated on one hemisphere of the nanoparticles,[9] and the close proximity between the ligands rendered it likely for the ligands to meet the topochemical principles for photopolymerization (Scheme 3).[14−16] Consequently, formation of dimers and trimers was apparent as manifested by their characteristic emission profiles. For BE nanoparticles, however, the DAT ligands were mixed rather homogeneously with the hexanethiolate ligands on the entire nanoparticle surface. Therefore, the surface dilution rendered it

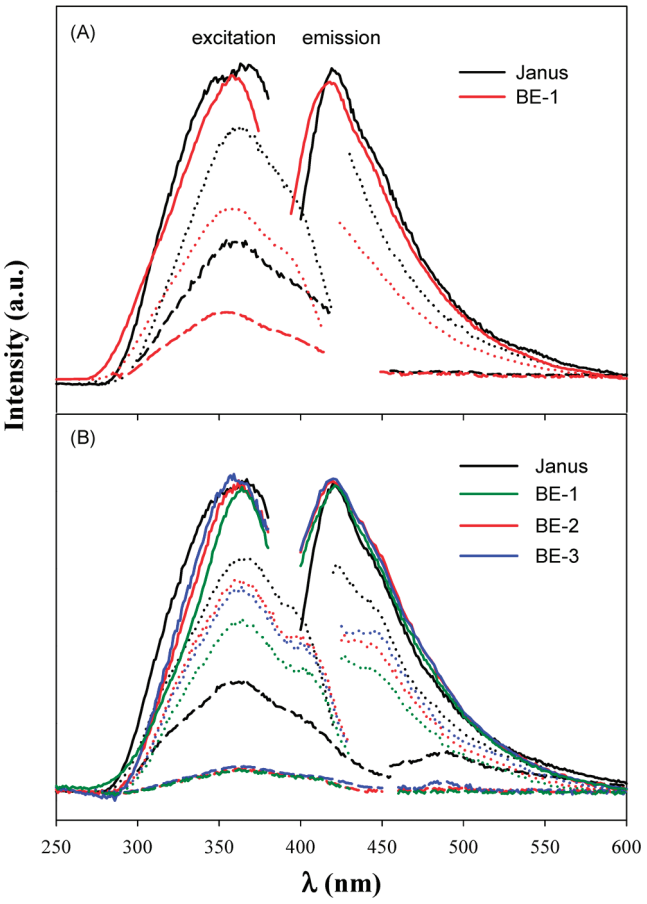

Figure 3. (A) Excitation and emission spectra of Janus (black curves) and BE-1 (red curves) nanoparticles before UV irradiation. (B) Excitaion and emission spectra of Janus and BE nanoparticles after UV irradiation: Janus, black curves; BE-1, green curves; BE-2, red curves; and BE-3, blue curves. Solid (—) curves were collected at λ_{ex} = 360 nm and λ_{em} = 420 nm, dotted (· · ·) curves were collected at λ_{ex} = 401 nm and λ_{em} = 445 nm, and dashed (---) curves were collected at λ_{ex} = 430 nm and λ_{em} = 485 nm. The particle concentrations were all ca. 0.5 mg/mL in THF.

difficult to have a large number of DAT ligands that were situated in close proximity. As a result, only dimers were produced, and higher orders of oligomers were formed only at significantly higher DAT surface coverages.

Importantly, the photoinduced cross-linking between the diacetylene moieties of neighboring DAT ligands led to marked enhancement of the structural integrity of the Janus nanoparticles. As mentioned earlier, mercapto derivatives on gold surfaces exhibit apparent surface diffusion even at ambient temperature. Therefore, the two types of ligands that were initially segregated on the Janus nanoparticle surface eventually became mixed rather homogeneously, analogous to the structure of BE nanoparticles. Yet, covalent cross-linking between the nanoparticle surface ligands is anticipated to help maintain the asymmetrical surface structure of the Janus nanoparticles. The hypothesis was proved by fluorescence measurements shown in Figure 4. It can be seen that for the Janus nanoparticles that had been subject to UV irradiation, after 30 days the three emission peaks remained well-defined at 419, 445, and 484 nm (black curves), and the relative intensity was virtually unchanged as compared to those before aging (Figure 3). In sharp contrast, when the Janus nanoparticles

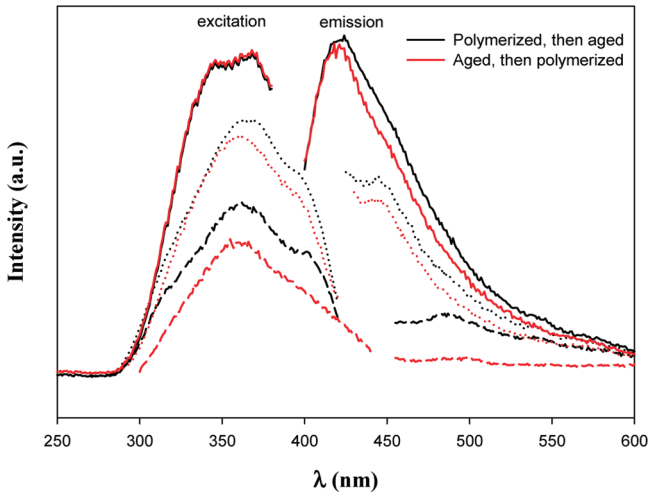

Figure 4. Excitation and emission spectra of Janus nanoparticles: black curves are the spectra collected where the nanoparticles were subject to UV irradiation and then were aged for 30 days, and red curves are those for the Janus nanoparticles that were aged for 30 days and then were exposed to UV lights. Solid (—) curves were collected at λ_{ex} = 360 nm and λ_{em} = 420 nm, dotted (· · ·) curves were collected at λ_{ex} = 401 nm and λ_{em} = 445 nm, and dashed (---) curves were collected at λ_{ex} = 430 nm and λ_{em} = 485 nm. The particle concentration was ca. 0.5 mg/mL in THF.

were first aged in solution at ambient temperature for 30 days and then were subject to UV irradiation, the intensity of the trimer emission was found to be minimal (red curves in Figure 4), and the overall fluorescence profiles became similar to those of BE nanoparticles (Figure 3), suggesting a structural evolution that most probably arose from the slow but apparent surface diffusion of monomeric thiol ligands on the nanoparticle surface.

CONCLUSION

In this study, Janus nanoparticles were prepared by taking advantage of the interfacial ligand-exchange reactions of hexanethiolate-protected gold nanoparticles with a mercapto derivative of diacetylene (with a terminal hydroxy functional group). ^{1}H NMR measurements showed that the protecting shell of the resulting nanoparticles consisted of ca. 50% hydrophobic hexanethiolates and 50% hydrophilic DAT ligands. Contact angle studies indicated that these two types of ligands were segregated on the two hemispheres of the nanoparticle surface, in contrast to the bulk-exchange counterparts. Consequently, the Janus nanoparticles behaved analogously to conventional surfactant molecules and could form stable superstructures in solvent media of varied polarity, as revealed in dynamic light scatterting measurements. Importantly, because of the close proximity of the diacetylene moieties on the Janus nanoparticle surfaces, exposure to UV irradiation led to effective covalent cross-linking between neighboring ligands, as manifested by the unique fluorescence characteristics of diacetylene dimers and trimers, in sharp contrast to bulk-exchange nanoparticles where the extent of ligand cross-linking was much limited as dictated by the topochemical principles for diacetylene polymerization. The cross-linking between the surface ligands also led to marked enhancement of the structural integrity of the Janus nanoparticles, as compared to unpolymerized Janus nanoparticles. This is critical in the further chemical functionalization and utilization of Janus nanoparticles.

dx.doi.org/10.1021/la2032626 |*Langmuir* 2011, 27, 14581–14588

■ ASSOCIATED CONTENT

Supporting Information. ^{1}H NMR spectra of the Janus and BE nanoparticles. This material is available free of charge via the Internet at http://pubs.acs.org.

■ AUTHOR INFORMATION

Corresponding Author
*E-mail: shaowei@ucsc.edu.

■ ACKNOWLEDGMENT

This work was supported by the National Science Foundation (DMR-0804049) and the ACS-Petroleum Research Fund (49137-ND10). The synthesis of the DAT ligand was performed as a User Project at the Molecular Foundry, Lawrence Berkeley National Laboratory, which was supported by the Office of Science, Office of Basic Energy Sciences, U.S. Department of Energy, under contract DE-AC02-05 CH11231.

■ REFERENCES

(1) Craighead, H. G. *Science* **2000**, *290*, 1532.
(2) Jager, E. W. H.; Smela, E.; Inganas, O. *Science* **2000**, *290*, 1540.
(3) Quake, S. R.; Scherer, A. *Science* **2000**, *290*, 1536.
(4) Zhang, Z. L.; Glotzer, S. C. *Nano Lett.* **2004**, *4*, 1407.
(5) Casagrande, C.; Fabre, P.; Raphael, E.; Veyssie, M. *Europhys. Lett.* **1989**, *9*, 251.
(6) Casagrande, C.; Veyssie, M. *C. R. Acad. Sci., Ser. II* **1988**, *306*, 1423.
(7) Pradhan, S.; Xu, L.; Chen, S. *Adv. Funct. Mater.* **2007**, *17*, 2385–2392.
(8) Xu, L. P.; Pradhan, S.; Chen, S. W. *Langmuir* **2007**, *23*, 8544–8548.
(9) Pradhan, S.; Brown, L. E.; Konopelski, J. P.; Chen, S. W. *J. Nanopart. Res.* **2009**, *11*, 1895–1903.
(10) Pradhan, S.; Ghosh, D.; Chen, S. W. *ACS Appl. Mater. Interfaces* **2009**, *1*, 2060–2065.
(11) Xu, Q.; Kang, X.; Bogomolni, R. A.; Chen, S. *Langmuir* **2010**, *26*, 14923–14928.
(12) Tsao, M. W.; Rabolt, J. F.; Schonherr, H.; Castner, D. G. *Langmuir* **2000**, *16*, 1734–1743.
(13) Jeschke, G.; Ionita, P.; Volkov, A.; Chechik, V. *Anal. Chem.* **2008**, *80*, 95–106.
(14) Enkelmann, V. *Structural aspects of the topochemical polymerization of diacetylenes*; Springer: Berlin/Heidelberg, Germany, 1984.
(15) Wegner, G. *Pure Appl. Chem.* **1977**, 443.
(16) Cao, G.; Mallouk, T. E. *J. Solid State Chem.* **1991**, *94*, 59–71.
(17) Menzel, H.; Mowery, M. D.; Cai, M.; Evans, C. E. *J. Phys. Chem. B* **1998**, *102*, 9550–9556.
(18) Alloisio, M.; Demartini, A.; Cuniberti, C.; Dellepiane, G.; Muniz-Miranda, M.; Giorgetti, E. *Vib. Spectrosc.* **2008**, *48*, 53–57.
(19) Brauer, G. *Handbook of preparative inorganic chemistry*, 2nd ed.; Academic Press: New York, 1963.
(20) Brust, M.; Walker, M.; Bethell, D.; Schiffrin, D. J.; Whyman, R. *J. Chem. Soc., Chem. Commun.* **1994**, 801–802.
(21) Alvarez, M. M.; Khoury, J. T.; Schaaff, T. G.; Shafigullin, M. N.; Vezmar, I.; Whetten, R. L. *J. Phys. Chem. B* **1997**, *101*, 3706–3712.
(22) Guo, R.; Song, Y.; Wang, G.; Murray, R. W. *J. Am. Chem. Soc.* **2005**, *127*, 2752–2757.
(23) Hostetler, M. J.; Templeton, A. C.; Murray, R. W. *Langmuir* **1999**, *15*, 3782–3789.
(24) Song, Y.; Murray, R. W. *J. Am. Chem. Soc.* **2002**, *124*, 7096–7102.
(25) Bohren, C. F.; Huffman, D. R. *Absorption and scattering of light by small particles*; Wiley: New York, 1983.
(26) Underwood, S.; Mulvaney, P. *Langmuir* **1994**, *10*, 3427–3430.
(27) Kim, T.; Crooks, R. M.; Tsen, M.; Sun, L. *J. Am. Chem. Soc.* **1995**, *117*, 3963–3967.
(28) Kim, T.; Ye, Q.; Sun, L.; Chan, K. C.; Crooks, R. M. *Langmuir* **1996**, *12*, 6065–6073.
(29) Menzel, H.; Mowery, M. D.; Cai, M.; Evans, C. E. *J. Phys. Chem. B* **1998**, *102*, 9550–9556.
(30) Kanaras, A. G.; Bartczak, D. *Langmuir* **2010**, *26*, 7072–7077.
(31) Warta, R.; Sixl, H. *J. Chem. Phys.* **1988**, *88*, 95–99.
(32) Miyano, K.; Maeda, T. *Phys. Rev. B* **1986**, *33*, 4386–4388.